PHYSICAL REVIEW C VOLUME 19, NUMBER 3 MARCH 1979

Total reaction cross sections and the matter density of finite nuclei

David J. Ernst
Physics Department, Texas A&M University, College Station, Texas 77843
(Received 27 July 1978)

A simple model for total reaction cross sections based on the impulse approximation and the use of an eikonal propagator is derived. Semiquantitative approximations are used to demonstrate that total reaction cross sections are determined by the radius at which the profile function is equal to one mean free path for the incident particle. A simple quantitative relation between the density and the profile function is also provided. The model is tested against existing data for proton-nucleus total reaction cross sections for ^{12}C, ^{16}O, $^{40,44,48}Ca$, and ^{208}Pb targets at energies from 100 MeV to 1 GeV. The total reaction cross sections are generally found to be in agreement (with several exceptions) with neutron densities determined either theoretically or from other experiments.

[NUCLEAR REACTIONS Total reaction cross sections, matter densities and radii.]

I. INTRODUCTION

The suggestion that total reaction cross sections at high energies could be used to measure the matter radii of nuclei is quite old.[1] The arguments were based on the optical analogy that for short wavelengths and a highly absorptive medium, the total reaction cross section σ_R approaches πR^2, where R is the radius of the target. For 1 GeV protons incident on a nucleus, the wavelength is about 0.7 fm, and the mean-free path of a proton in nuclear matter is about 1.3 fm. Thus one has a short wavelength and a highly absorptive medium, and the old models are indeed qualitatively correct. In addition, if we take the proton densities from electron scattering, total reaction cross sections can be used to study the contribution of neutrons to the matter density.

The purpose of this work is to derive a quantitative model which makes use of the wavelength of the incident nucleon and its mean-free path as small parameters. Such a model results from using what are quite standard approximations. The model is applied to existing data to see if they may be used to determine properties, such as the rms radius, of a nucleus. In addition, we examine in some detail the question of exactly what properties of the nuclear density determine the total reaction cross section.

In Sec. II we derive a simple formula for the total reaction cross section utilizing the following approximations:

(1) The scattering can be described by a first order optical potential in the impulse approximation.

(2) The eikonal propagator can be used to solve the Lippmann-Schwinger equation for the scattering from the optical potential.

Each of these approximations is commonly employed at 1 GeV, and the corrections to them should be quite small.

In Sec. III, some semiquantitative approximations are used to determine which aspects of the nuclear density determine total reaction cross sections. It is found that σ_R is approximately $\pi R_{\rm eff}^{\ 2}$ where $R_{\rm eff}$ is the radius at which the profile function is equal to one mean-free path for the incident particle. The profile function is, in turn, shown to be determined by the nuclear density and its radial derivative at the half density point. Thus, total reaction cross sections are found to be sensitive to the nuclear density in a region near this effective radius.

This radius is generally larger than the half density radius of the nucleus; therefore σ_R is entirely determined by the tail of the nuclear density. That $R_{\rm eff}$ is larger than the geometrical radius of a nucleus has also been found[2] in the study of pion-nucleus total cross sections. In both cases, the reason is simply that the two-body interaction is sufficiently strong (i.e., the mean-free path is sufficiently short) that the projectile interacts strongly with the tail of the nucleus and seldom penetrates in even as far as the half density point.

In Sec. IV, the model is compared with the existing data for σ_R from 100 MeV to 1 GeV for ^{12}C, ^{16}O, $^{40,44,48}Ca$, and ^{208}Pb. It is found that the model seems to work very well, even down to energies of nearly 100 MeV. As corrections to the model (especially corrections to the use of an eikonal propagator and the second order corrections to the optical potential) are expected to be substantial at this low an energy, it is not understood why the calculated results are good down to such a low en-

ergy. In general, total reaction cross sections are found to be consistent with densities determined by high energy elastic proton scattering. In two cases, ^{40}Ca and ^{208}Pb, the total reaction cross sections indicate that Hartree-Fock calculations underestimate slightly the number of neutrons in the tail region of these nuclei. For ^{48}Ca, the total reaction cross section indicates a larger neutron radius than is found in other experiments.

II. DERIVATION OF MODEL

We begin by assuming that the elastic scattering of a nucleon from a nucleus can be described by an optical potential[3] in the impulse approximation. In momentum space this gives, for the optical potential

$$(\vec{k}\,|U|\,\vec{k}) = A\int d\vec{p}\,(\vec{k}' - \vec{p} - \tfrac{1}{2}\vec{k}\,|\,t\,|\,\vec{k} - \vec{p} - \tfrac{1}{2}\vec{k}') \times \rho\left(\vec{p} + \frac{\vec{k} - \vec{k}'}{2}, \vec{p} - \frac{\vec{k} - \vec{k}'}{2}\right), \quad (2.1)$$

where $(\vec{k}'|\,t\,|\vec{k})$ is the T matrix for the elastic scattering of two nucleons from an initial relative momenta $\vec{k}$ to a final relative momenta $\vec{k}'$. The function $\rho(p', p)$ is the usual off-diagonal single particle density function. It is often assumed that $(\vec{k}'|\,t\,|\vec{k})$ is a local operator, i.e., $(\vec{k}'|\,t\,|\vec{k}) = t(|\vec{k}' - \vec{k}|)$, in which case the t matrix comes out of the fermi integration in (2.1). This factorization can, however, be justified under the more general argument[4] that the size of the two-body interaction (in coordinate space) is much smaller than the nuclear size. In Ref. 5, it is shown that this implies that the density function ρ in (2.1) restricts the value of $\vec{p}$ in the integration to values which are approximately zero. We may, therefore, remove the T matrix from the integration if we evaluate it at $\vec{p} = 0$,

$$(\vec{k}'|U|\,\vec{k}) = A\left(\vec{k}' - \frac{\vec{k} + \vec{k}'}{4}\,|\,t\,|\vec{k} - \frac{\vec{k}' + \vec{k}}{4}\right)\rho(\vec{k} - \vec{k}'), \quad (2.2)$$

where $\rho(q)$ is the Fourier transform of the single particle density. It is also shown in Ref. 5 that the next correction to this factorization (of order $|\vec{k}' - \vec{k}|/M$) is identically zero.

If we rewrite the dependence of $(\vec{k}\,|\,t\,|\vec{k})$ on $\vec{k}'$ and $\vec{k}$ as

$$(\vec{k}'|\,t\,|\vec{k}) = t\left(\frac{\vec{k}' + \vec{k}}{2}, \vec{k}' - \vec{k}\right), \quad (2.3)$$

then $\rho(\vec{k} - \vec{k}')$ restricts us to the region $\vec{k}' \cong \vec{k}$. Thus we may approximate

$$(\vec{k}'|\,t\,|\vec{k}) \cong t(\vec{k}, \vec{k}' - \vec{k}) \equiv \tilde{t}_E(\vec{k}' - \vec{k}) \quad (2.4)$$

to achieve

$$(\vec{k}'|U|\,\vec{k}) = U_E(\vec{k}' - \vec{k}) = A\tilde{t}_E(\vec{k}' - \vec{k})\,\rho(\vec{k}' - \vec{k}). \quad (2.5)$$

This is a quite standard approximation to the optical potential; it is rederived here only to demonstrate that it does not depend on the assumption that the two-body T matrix is a function of momentum transfer only, or even that its predominant dependence is on momentum transfer. It obtains more generally from the fact that the size of the two-body interaction is smaller than the size of the target.

Since we are interested in scattering at high energies, we may make use of the eikonal approximation to express the wave function for the scattering from the potential (2.2) as

$$\psi_E^{(+)}(\vec{r}) = \psi_E^{(+)}(z, \vec{b}) = \frac{e^{ikz}}{(2\pi)^{3/2}} \exp\left[-\frac{i}{\hbar v}\int_{-\infty}^{z} U(\vec{b}, z')\,dz'\right], \quad (2.6)$$

where z is the component of $\vec{r}$ along the incident direction, $\vec{b}$ is a vector perpendicular to z, and $U(r)$ is the Fourier transform of $U(q)$. We may then use the unitarity relation for scattering from a non-Hermitian potential,

$$\sigma_R(E) = \frac{16\pi^3 m}{\hbar^2 k}\int d\vec{r}\,\psi_E^{(+)\dagger}(\vec{r})\,\mathrm{Im}U_E(\vec{r})\,\psi_E^{(+)}(\vec{r}), \quad (2.7)$$

together with (2.6) to get[6]

$$\sigma_R(E) = \int d^{(2)}b\left[1 - \exp\left(\frac{2}{\hbar v}\int_{-\infty}^{+\infty}\mathrm{Im}U_E(\vec{b}, z')\,dz'\right)\right]. \quad (2.8)$$

If we further note that

$$\mathrm{Im}\tilde{t}_E(\vec{k}' - \vec{k}) = -\frac{k\hbar^2}{2m}\sigma_{\mathrm{tot}}(E)\,f(\vec{k}' - \vec{k}), \quad (2.9)$$

with $f(0) = 1$ and σ_{tot} is the total nucleon-nucleon cross section, we find

$$\sigma_R(E) = \int d^{(2)}b\left\{1 - \exp\left[-\int_{-\infty}^{+\infty}(Z\sigma_{pp}\tilde{\rho}(z, \vec{b}) + N\sigma_{pn}\tilde{\rho}_n(z, b))dz'\right]\right\}, \quad (2.10)$$

where we have used subscripts p or n to distinguish between the protons and neutrons in the target. The modified density $\tilde{\rho}_i(r)$ which appears in (2.10) is the point nucleon density folded with the nucleon-nucleon interaction,

$$\tilde{\rho}_i(\vec{r}) = \int d\vec{r}' f(\vec{r} - \vec{r}')\rho_i(\vec{r}'), \tag{2.11}$$

with $f(\vec{r})$ the Fourier transform of $f(\vec{q})$ defined in (2.9).

This result, (2.10) and (2.11), is more valid than one might naively believe. The corrections to this formula are the following:

(1) The inclusion of higher order terms in the optical potential. At energies near 1 GeV these corrections have been found to be quite small,[7] especially near the forward direction. The second order term should increase[8] as the energy decreases, and it is not at all clear how large the second order will be at energies as low as 100 MeV.

(2) Corrections to the use of the free nucleon-nucleon T matrix should be considered. One would expect the chief correction here to be the Pauli blocking[3] effect; the free T matrix should be replaced by the Bethe-Goldstone reaction matrix. The exact size of this effect for nucleons at intermediate energies has not been determined. An alternative approach might be to use the KMT pseudo-optical potential[9] because this potential, in the impulse approximation, requires only the free T matrix. However, we have used the unitarity relation to derive our final result, and the KMT method of scaling the scattering operators by $A/(A-1)$ prevents one from using simple unitarity[10] arguments.

III. SEMIQUANTITATIVE ARGUMENTS

In this section, we develop some approximations which have been found to be accurate to within 1 to 5%. The purpose of developing these approximations is not to aid in performing the numerical work necessary to calculate σ_R from the formulas in the previous section, but more to try to illuminate exactly what aspects of the target determine σ_R.

We begin by examining the folding integral in Eq. (2.11). We shall assume a Gaussian form for $f(\vec{r})$,

$$f(\vec{r}) = e^{-r^2/\beta^2}, \tag{3.1}$$

which is equivalent to assuming

$$(\vec{k}'|\,t\,|\vec{k}) = t(0)\exp[-\beta^2(\vec{k} - \vec{k}')^2/2]\,. \tag{3.2}$$

We repeat that one is not assuming that $(\vec{k}'|\,t\,|\vec{k})$ behaves in this manner over any extended region; we require only that this be a satisfactory parametrization of the T matrix in the very limited region $\vec{k} \cong \vec{k}'$.

In Eq. (2.4), one should also include the spin dependent piece of the nucleon-nucleon interaction which would then give rise to a spin-orbit term in the optical potential. This term is important[11] if one is interested in detailed behavior of differential cross sections; it, however, contributes less than a percent to total cross sections (except[11] for He, where it contributes 4% to the total cross section). We shall, therefore, ignore it.

With this parametrization of the two-body T matrix, we may rewrite Eq. (2.11) for the folded density as,[12] after some algebra,

$$\tilde{\rho}(r) = \pi^{-1/2}\int_{-\infty}^{+\infty} e^{-u^2}\rho(r + \sqrt{2}\,\beta u)\,du + \left(\frac{2}{\pi}\right)^{1/2}\frac{\beta}{r}\int_0^{\infty} e^{-w}[\rho(r + \beta\sqrt{2w}) - \rho(r - \beta\sqrt{2w})]\,dw\,. \tag{3.3}$$

A two-point Gauss-Hermite integration for the first integral and one point Gauss-Laguerre integration for the second integral yields the following approximation:

$$\tilde{\rho}(r) = \tfrac{1}{2}[\rho(r+\beta) + \rho(r-\beta)] + (2\pi)^{-1/2}\frac{\beta}{r}[\rho(r + \sqrt{2}\,\beta) - \rho(r - \sqrt{2}\,\beta)]\,. \tag{3.4}$$

In all cases examined (densities from ^{12}C through ^{208}Pb), this approximation has been found to be accurate to better than 1%.

The qualitative difference between the folded density $\tilde{\rho}(r)$ and the point density $\rho(r)$ can be found by parametrizing both $\tilde{\rho}(r)$ and $\rho(r)$ as fermi functions,

$$\rho(r) = \rho_0\left[1 + \exp\left(\frac{r - R}{a}\right)\right]^{-1} \tag{3.5}$$

and

$$\tilde{\rho}(r) = \tilde{\rho}_0\left[1 + \exp\left(\frac{r - \tilde{R}}{\tilde{a}}\right)\right]^{-1}. \tag{3.6}$$

We then expand Eq. (3.4) with these explicit parametrizations of $\rho(r)$ and $\tilde{\rho}(r)$ about $r = R$ and match coefficients in the expansion. We obtain the following estimates of the folded density parameters:

$$\tilde{a} = a\,\frac{y(1-y)}{z} \tag{3.7}$$

and

$$\tilde{R} = R - \tilde{a}\ln\left(\frac{1-y}{y}\right), \tag{3.8}$$

with

$$y = \frac{1}{2}\left\{1 + \left(\frac{2}{\pi}\right)^{1/2}\frac{\beta}{R}\left[\frac{1-\exp(\sqrt{2}\beta/a)}{1+\exp(\sqrt{2}\beta/a)}\right]\right\} \tag{3.9}$$

and

$$z = [\exp(\beta/a)]/[1+\exp(\beta/a)]^2. \tag{3.10}$$

From Eq. (3.7), we find that the folding of the nucleon-nucleon amplitude with the density increases the skin thickness a. For a large nucleus and commonly used values of β ($\beta \sim a$), the increase in the skin thickness is approximately 20%.

From Eq. (3.8) we find that the folding of the density with the nucleon-nucleon amplitude actually *decreases* the half density radius by a small amount. This contradicts several comments in the literature where it seems to have been assumed that the folding would increase the radius. We have, therefore, checked this result numerically by integrating Eq. (3.3) and then fitting a fermi function to the resulting $\tilde{\rho}(r)$. The results were quite close to those obtained from Eqs. (3.7)–(3.10).

The reason for the decrease in the radius is purely geometrical and can be understood by considering the overlap of two spheres of radius R_1 and R_2 as depicted in Fig. 1. We first notice that the interaction is written in terms of r, the distance between the centers of two finite spheres, and that the interaction is proportional to the overlap of the two spheres. Thus there is no overlap and no interaction for r greater than R_1+R_2. There is a maximum overlap and interaction when r is less than R_1-R_2. When $r=R_1$, the radius of the larger sphere, the overlap is *less* than half as can be seen in Fig. 1(a); it is not until r is slightly less than R_1 that one finds that half of the volumes of the two spheres overlap, as depicted in Fig. 1(b). The geometrical reason for this decrease in the half density radius has been known

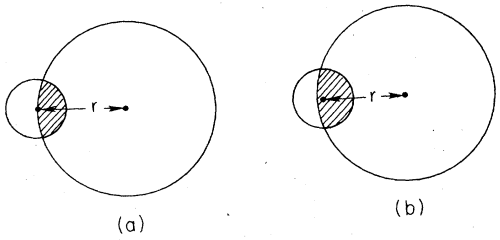

FIG. 1. The overlap of two spheres demonstrates geometrically why the half density radius of the folded density is slightly smaller than the half density radius of the point density.

for the deuteron-nucleus folding model[13] where the decrease in radius is much larger because of the large size of the deuteron. The decrease in radius here is much smaller, but the argument is still valid.

The next problem one must consider is that scattering is not determined by the density $\tilde{\rho}(r)$ but rather by the profile function which occurs in Eq. (2.10),

$$S(b) = \frac{1}{\tilde{\rho}(0)}\int_{-\infty}^{+\infty}\tilde{\rho}(z', b)\,dz', \tag{3.11}$$

where, for simplicity, we have set $\sigma_{pn}=\sigma_{pp}$ and $\tilde{\rho}_p(r)=\tilde{\rho}_n(r)$. The function $S(b)$ is simply the amount of matter one encounters while passing through the nucleus on a straight line path a distance b from the center. Rewriting Eq. (3.11) in polar coordinates and integrating by parts gives

$$S(b) = \frac{2}{\tilde{\rho}(0)}\int_0^{\infty}(r^2-b^2)^{1/2}\left[\frac{d\tilde{\rho}(r)}{dr}\right]dr. \tag{3.12}$$

This formula is quite useful as $d\tilde{\rho}(r)/dr$ is a sharply peaked function at some point in the nuclei surface r_0 and thus $S(b)$ will be approximately proportional to $(r_0^2-b^2)^{1/2}$. The theory of Gaussian integration tells one which is the best single point r_0 for evaluating this integral; we need only to define $d\tilde{\rho}(r)/dr$ as the weight function for the integration, construct the lowest two orthogonal polynomials on this weight function, then r_0 is just the zero of the second polynomial. If we choose $\tilde{\rho}(r)$ to be a fermi function, Eq. (3.6), then $S(b)$ is found to be

$$S(b) = 2[r_0^2(b)-b^2]^{1/2}\tilde{\rho}(b)/\tilde{\rho}(0), \tag{3.13}$$

with $r_0(b)$ given by

$$r_0(b) = b - \frac{1}{2}\left[\frac{\tilde{\rho}(r)}{(d\tilde{\rho}(r)/dr)}\bigg|_{r=\tilde{R}}\right]\frac{\tilde{\rho}(0)}{\tilde{\rho}(b)} \times\ln\left(1-\frac{\tilde{\rho}(b)}{\tilde{\rho}(0)}\right). \tag{3.14}$$

The use of Eqs. (3.13) and (3.14) to generate a profile function from a density has been examined numerically, and it was found that they are accurate to better than 2% unless one is in a region where $\tilde{\rho}(r)$ is itself quite small (less than 5% its central value).

These equations, therefore, provide a reasonably simple and quantitative approximation to the profile function; they also show that the relationship between the density and the profile function is rather complex. Since scattering experiments measure most directly the profile function, one must be quite cautious in deducing properties of the density. One can, however, note the following from these equations: (1) In the interior of a nu-

cleus where $\tilde{\rho}(b)$ is constant, $S(b) \approx 2(\tilde{R}^2 - b^2)^{1/2}$, the result for a square density of radius $\tilde{R}$. (2) $S(b)$ is proportional to $\tilde{\rho}(b)$, the proportionality factor being the square root function in Eq. (3.14). (3) In the surface region $r_0(b)$ is a complicated function of b, but we can see that this function depends very sensitively on the derivative of the density at the half density point (i.e., the skin thickness).

Finally, we examine the calculation of the total reaction cross section from the profile function via Eq. (2.10), which for $\tilde{\rho}_p = \tilde{\rho}_n$ and $\sigma_{np} = \sigma_{nn}$ becomes

$$\sigma_R(E) = 2\pi \int_0^\infty b\, db \left[1 - \exp\left(-\frac{S(b)}{\lambda}\right)\right], \tag{3.15}$$

with λ equal to the mean-free path defined by

$$\lambda \equiv [A\tilde{\rho}(0)\sigma]^{-1}. \tag{3.16}$$

Integrating (3.15) by parts gives

$$\sigma_R(E) = \pi \int_0^\infty b^2\, db \left[\frac{d}{db} \exp\left(\frac{S(b)}{\lambda}\right)\right]. \tag{3.17}$$

Now if one considers S the independent variable and b becomes $b(S)$ the dependent variable, this becomes

$$\sigma_R(E) = \pi \int_0^\infty b^2(S)\, e^{-S/\lambda} \frac{dS}{\lambda}. \tag{3.18}$$

A one point Gauss-Laguerre integration provides us with the approximation

$$\sigma_R(E) = \pi R_{\text{eff}}^{\,2}, \tag{3.19}$$

where R_{eff} is the effective radius given by the relation

$$S(R_{\text{eff}}) = \lambda. \tag{3.20}$$

Thus the total reaction cross section is given in terms of the radius at which the profile function is equal to one mean-free path.

The use of Eq. (3.19) to approximate Eq. (3.15) has been checked numerically and in all the cases examined the approximation underestimates $\sigma_R(E)$ by about 5%. This is because the one point integration of Eq. (3.18) ignores the contribution from the long range tail of $S(b)$.

In the next section, we shall find that R_{eff} is larger than the half-density radius. Thus the incident proton does not significantly penetrate even in as far as the half-density point. The reaction cross sections are determined by the density in the tail region. For this reason the older models which were based on a square density (which is identically zero beyond the half-density radius) cannot be quantitatively correct.

IV. REACTION CROSS SECTIONS FOR ^{12}C, ^{16}O, ^{40,44,48}Ca, ^{208}Pb

In this section we compare total reaction cross sections predicted by the model developed in Sec. II with existing data. We calculate $\sigma_R(E)$ numerically from Eqs. (2.10) and (2.11). The approximations given in Eqs. (3.4), (3.13), and (3.19) are not used here. They provide a simple and easy way of calculating $\sigma_R(E)$ but yield results which are in error by about 5%. The use of Eqs. (2.10) and (2.11) requires a straightforward three dimensional integration and, from the arguments given in Sec. II, one would expect these results to be quite accurate.

First, we examine the case of ^{12}C; for such a light target, the simple formulas based on a square density are not even qualitatively[14] correct. In Ref. 15 formulas similar to those used here but based upon an α-particle model of ^{12}C were found to be in agreement with the measured reaction cross sections.

We assume that $\tilde{\rho}_n = \tilde{\rho}_p$ and may be obtained directly from electron scattering data[16] as

$$\tilde{\rho}_p(r) = 0.08371 \left[1 + \frac{4}{3}\left(\frac{r}{b}\right)^2\right] \exp\left[-\left(\frac{r}{a}\right)^2\right], \tag{4.1}$$

with $b = 1.705$ fm and $a = 1.649$ fm. The use of $\tilde{\rho}(r)$ directly from electron scattering data assumes the electron-nucleon form factor has a range factor in Eq. (3.1) equal to the size of the proton-proton and proton-neutron interaction. This is a reasonably accurate assumption as these parameters are close and the reaction cross section does not depend very sensitively on the exact choice of the range. We could have used a more accurately determined density,[17] but to within the errors quoted on the reaction cross sections, Eq. (4.1) is sufficient. The nucleon-nucleon total cross sections which we require are found from interpolating between the experimental points of Ref. 18. The resulting $\sigma_R(E)$ for laboratory proton energies from 100 to 900 MeV are depicted in Fig. 2 together with the available experimental numbers.[14,19-24] The agreement is quite satisfactory and there is no need to invoke an α-particle[15] model of ^{12}C to understand these data.

The results, both experimental and theoretical, for ^{16}O are also given in Fig. 2. The densities $\tilde{\rho}_n$ and $\tilde{\rho}_p$ are constructed from Negele's density dependent Hartree-Fock densities[25] via Eq. (2.11) with[26] $\beta_p = 0.442$ fm and $\beta_n = 0.542$ fm in Eq. (3.1). Again, we agree satisfactorily with the measured cross sections.

As there has been much interest lately in the

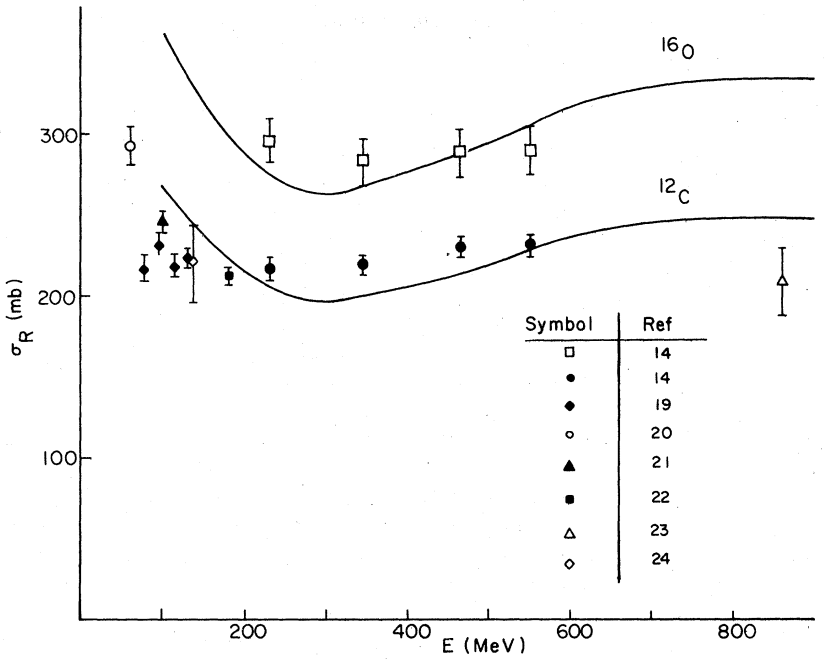

FIG. 2. The total reaction cross section for ^{16}O and ^{12}C calculated from the model developed here and some of the available data. The open squares (□) are data from Ref. 14 for ^{16}O. The solid circles (●) and all other data are for ^{12}C.

location of the neutrons in the Ca isotopes, we have calculated $\sigma_R(E)$ for ^{40}Ca, ^{44}Ca, and ^{48}Ca. We have used $\tilde{\rho}_n$ and $\tilde{\rho}_p$ as determined from elastic proton-nucleus scattering in Ref. 27. These results are the dashed lines in Fig. 3. We have also calculated $\tilde{\rho}_p$ and $\tilde{\rho}_n$ from Negele's[25] densities (as was done with ^{16}O) and these results are depicted in Fig. 3 as the solid lines. We see that the two densities for ^{48}Ca (in the region of the tail where there is sensitivity) are in good agreement with each other, whereas the ^{40}Ca density determined from elastic proton scattering contains slightly more neutrons in the tail than does the Hartree-Fock density. The recently measured[28] reaction cross sections at 700 MeV are in excellent agreement with the densities for ^{40}Ca and ^{44}Ca determined from elastic proton scattering. The reaction cross section for ^{48}Ca, however, is in disagreement with both densities. If the proton density is taken from electron scattering, while

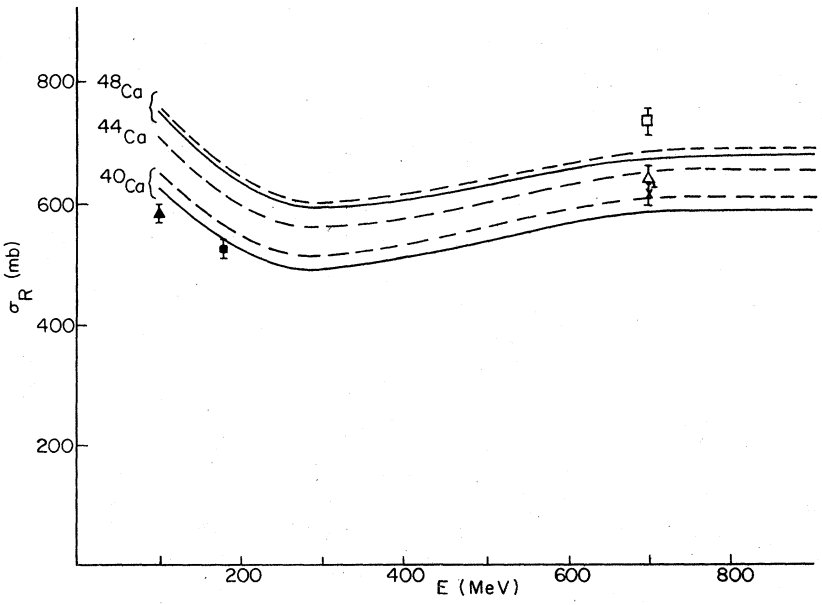

FIG. 3. The total reaction cross sections for the Ca isotopes. The solid lines represent calculations utilizing the Hartree-Fock densities from Ref. 25, while the dashed lines use densities from Ref. 27. The experimental points at 700 MeV for each of the isotopes are from Ref. 28; the open square (□) is for ^{48}Ca, the open triangle (△) is for ^{44}Ca, and the X is for ^{40}Ca. The two low energy points are for ^{40}Ca with the data key given in Fig. 2.

TABLE I. The difference in the matter radii of Ca isotopes.

Particle	Ref.	^{44}Ca $\langle r_m^{44}\rangle - \langle r_m^{40}\rangle$ (fm)	^{48}Ca $\langle r_m^{48}\rangle - \langle r_m^{40}\rangle$ (fm)
79 MeV α	29		0.05 ± 0.04
90–240 MeV $\pi^{\pm}$	30	0.01 ± 0.04	0.053 ± 0.04
1.37 GeV α	31	0.09 ± 0.035	0.12 ± 0.035
1 GeV p	27		0.15 ± 0.02
Hartree-Fock	25		0.19
166 MeV α	32	0.17 ± 0.20	0.38 ± 0.17
15 MeV p	33	0.01 ± 0.09	0.22 ± 0.09
700 MeV p	This work	0.05 ± 0.09	0.36 ± 0.09

the neutron density is taken to be a wine-bottle shape and then $\tilde{R}$ or $\tilde{a}$ is increased until the calculated cross section agrees with the measured cross section, the neutron-proton difference for ^{40}Ca ($\langle r_n^2\rangle^{1/2} - \langle r_p^2\rangle^{1/2}$) is found to be -0.045 ± 0.11 in excellent agreement with Hartree-Fock predictions (−0.04 fm) and elastic proton scattering measurements (−0.07 fm). For ^{44}Ca this difference is found to be 0.01 ± 0.11 fm which is also in agreement[30-32] with other determinations.

Total reaction cross sections most directly measure the difference in matter radii. The difference in matter radii for ^{48}Ca and ^{40}Ca, and for ^{44}Ca and ^{40}Ca, determined from this fit to total reaction cross sections is presented[34] in Table I together with other determinations of this quantity. The total reaction cross section for ^{48}Ca indicates a need for more neutrons in the tail. One should notice, however, that the Hartree-Fock value is 2 standard deviations from our experimentally determined value. Thus, the discrepancy might be statistical in nature and additional work on this point is probably required. There is also a model dependence[35] in how one extracts matter radii from the data.

From Eqs. (3.19), (3.20), and (3.13) we can see that the reaction cross sections are predominantly determined by the density (and its derivative) near the radius R_{eff}. The measured reaction cross sections yield a radius of 4.42 fm, 3.51 fm, and 4.84 fm for ^{40}Ca, ^{44}Ca, and ^{48}Ca respectively. These are to be compared with $R = 1.2\ \text{fm} \times A^{1/3}$ of 4.10 fm, 4.24 fm, and 4.36 fm. Thus, the reaction cross sections are being determined by the density at a radius several tenths of a fermi beyond the half density point. It is the assumption of a wine-bottle shape for the densities which allows one to infer an rms radius from the measurement of the

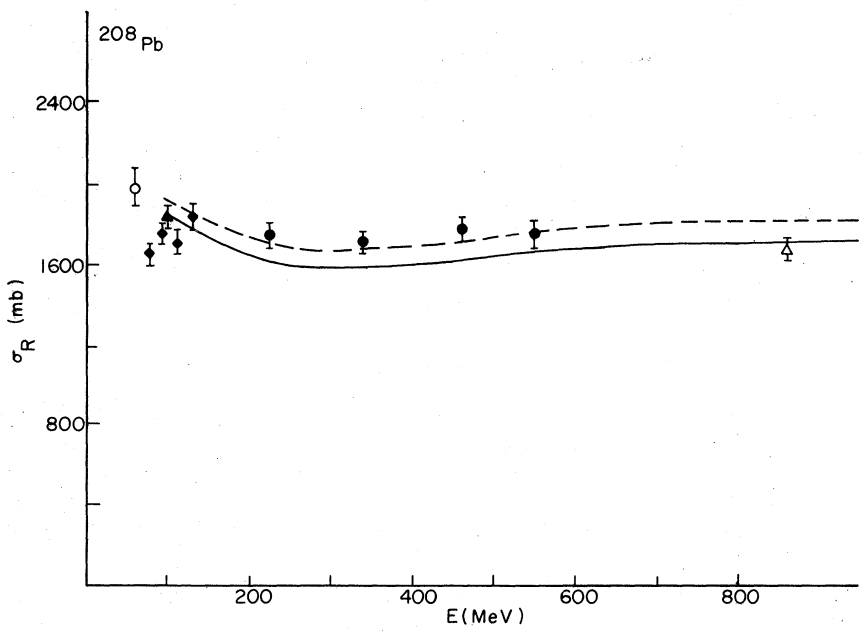

FIG. 4. The total reaction cross sections for ^{208}Pb. The data key is given in Fig. 2.

density in the tail.

In Fig. 4, we present the results for ^{208}Pb. Again the dashed curve represents calculations using $\tilde{\rho}_n$ and $\tilde{\rho}_p$ from Ref. 21, while the solid curve represents calculations done by folding the Hartree-Fock density[25] with the nucleon-nucleon interaction. If we concentrate on the more recent experimental points,[14] we see that densities from Ref. 27 are in excellent agreement with measured reaction cross sections. The Hartree-Fock density produces reaction cross sections which are consistently a small amount low. To agree with the elastic scattering data and the total reaction cross sections there is a need for a slight *increase* in the number of neutrons in the tail of the density.

At first glance, this contradicts the statement of Ref. 27 where they state that their density requires that the difference in the neutron and proton rms radii be *decreased*. They, however, varied a matter density in order to fit the elastic proton scattering data and then infer a neutron radius. Such an approach is probably quite model dependent as the effective radius defined in Eq. (3.20) is about 7.5 fm. It is the density in this region which determines the reaction cross sections (and to a great extent, the elastic scattering); in this region, the density of Ref. 27 has *more* neutrons than does the Hartree-Fock density.

This exemplifies the difficulty[35] of trying to use a surface dominated reaction to determine a global property of a nucleus, such as the rms radius. It is perhaps better to use the total reaction cross sections and elastic scattering data to constrain the density near R_{eff}, as the arguments in Sec. II have shown that this is actually what is being determined.

V. CONCLUSIONS

We have found that total reaction cross sections can be understood in terms of a simple model. Being only a single number at a particular energy, they do not, of course, contain as much information as the elastic differential cross section. The theoretical analysis of reaction cross sections is, however, sufficiently unencumbered by corrections that their measurement does provide an additional constraint on the matter density of a nucleus.

In particular, we have found that the existing reaction cross section data for ^{12}C, ^{16}O, and ^{44}Ca is in reasonable agreement with other determinations of these densities. For ^{40}Ca and ^{208}Pb, the reaction cross sections are in agreement with densities determined from elastic proton scattering. In these two cases, however, the reaction cross sections and the elastic proton scattering data indicate the need in Hartree-Fock calculations for a slight increase in the number of neutrons in the surface. The recent datum[28] for ^{48}Ca indicates a larger neutron radius than is found from elastic proton scattering or in the Hartree-Fock calculations.

This work was supported in part by the National Science Foundation.

[1]S. Fernbach, R. Serber, and T. B. Taylor, Phys. Rev. 75, 1352 (1949); H. A. Bethe, *ibid.* 57, 1125 (1940).
[2]A. S. Carroll, I -H. Chiang, C. B. Dover, T. F. Kycia, K. L. Li, P. O. Mazur, D. N. Michael, P. M. Mockett, D. C. Rahm, and R. Rubinstein, Phys. Rev. C 14, 635 (1976); K. McVoy, Nucl. Phys. A276, 491 (1977); M. D. Couper and M. B. Johnson, *ibid.* A260, 352 (1976); J. E. Sedlak and W. A. Friedman, report (unpublished).
[3]K. M. Watson, Phys. Rev. 89, 575 (1953).
[4]An alternative argument would be to use a unitary transform to render the t matrix a function of momentum transfer only; see J. F. Reading, Phys. Rev. C 1, 936 (1970).
[5]D. J. Ernst and G. A. Miller, (unpublished).
[6]R. J. Glauber, *Lectures in Theoretical Physics*, edited by W. E. Brittin and L. G. Dunham (Interscience, New York, 1959) Vol. 1.
[7]H. Feshbach and J. Hufner, Ann. Phys. (N.Y.) 56, 268 (1970); H. Feshbach, A. Gal, and J. Hufner, *ibid.* 66, 20 (1971); E. Lambert and H. Feshback, *ibid.* 76, 80 (1973).
[8]D. J. Ernst, J. T. Londergan, G. A. Miller, and R. M. Thaler, Phys. Rev. C 16, 537 (1977).
[9]A. Kerman, H. McManus, and R. Thaler, Ann. Phys. (N.Y.) 8, 551 (1959).
[10]D. J. Ernst, C. M. Shakin, and R. M. Thaler, Phys. Rev. C 9, 1374 (1974).
[11]E. Kujawski and J. P. Vary, Phys. Rev. C 12, 1271 (1975).
[12]J. W. Wilson and C. M. Costner, report (unpublished).
[13]W. F. Junkin and F. Villars, Ann. Phys. (N.Y.) 45, 93 (1967); 51, 68 (1969).
[14]P. U. Renberg, D. F. Measday, M. Pepin, P. Schwaller, B. Favier, and C. Richard-Serre, Nucl. Phys. A183, 81 (1972).
[15]I. Ahmad and Z. A. Khan, Nucl. Phys. A274, 519 (1976).
[16]I. Sick and J. S. McCarthy, Nucl. Phys. A150, 631 (1970).
[17]J. L. Friar and J. W. Negele, Nucl. Phys. A240, 301 (1975).
[18]D. V. Bugg, D. C. Saltoe, G. H. Stafford, R. F. George, K. F. Riley, and R. J. Tapper, Phys. Rev. 146, 980 (1966).
[19]R. Goloskie and K. Strauch, Nucl. Phys. 29, 474 (1962).
[20]J. J. H. Menet, E. E. Gross, J. J. Malanify, and A. Zucker, Phys. Rev. Lett. 22, 1128 (1969).

[21]P. Kirby and W. T. Link, Can. J. Phys. 44, 1847 (1966).
[22]A. Johansson, U. Svanberg, and O. Sundberg, Ark. Fys. 19, 527 (1961).
[23]F. F. Chen, C. P. Leavitt, and A. M. Shapiro, Phys. Rev. 99, 857 (1955).
[24]J. M. Cassels and J. D. Lawson, Proc. Phys. Soc. London 67, 125 (1954).
[25]J. W. Negele, Phys. Rev. C 1, 1260 (1970).
[26]A. Chameaux, V. Layly, and R. Schaeffer, Phys. Lett. 72B, 33 (1977).
[27]G. K. Varma and L. Zamick, Phys. Rev. C 16, 308 (1977); G. D. Alkhazov, T. Bauer, R. Beurty, A. Boudard, G. Bruge, A. Chameaux, P. Couvert, G. Cvijanovich, H. H. Duhm, J. M. Fontaine, D. Garreta, A. V. Kulikov, D. Legrand, J. C. Lugol, J. Saudinos, J. Thirion, and A. A. Vorobyov, Nucl. Phys. A274, 443 (1976).
[28]B. D. Anderson, P. R. Bevington, F. H. Cverna, M. W. McNaughton, R. J. Barrett, N. S. P. King, and D. J. Ernst, companion paper, Phys. Rev. C 19, 905 (1979).
[29]G. M. Lerner, J. C. Hiebert, L. L. Rutledge, Jr., C. Papanicolas, and A. M. Bernstein, Phys. Rev. C 12, 778 (1975).
[30]M. J. Jakobson, G. R. Burleson, J. R. Calarco, M. D. Cooper, D. C. Hagerman, I. Halpern, R. H. Jeppeson, K. F. Johnson, L. D. Kuitson, R. E. Marrs, H. O. Meyer, and R. P. Redwine, Phys. Rev. Lett. 38, 1201 (1977).
[31]G. D. Alkhazov, T. Bauer, R. Bertini, L. Binbot, O. Bing, A. Boudard, G. Bruge, H. Catz, A. Chamaux, P. Couvert, J. M. Jontaine, F. Hibou, G. J. Igo, J. C. Lugol, and M. Matoba, Nucl. Phys. A280, 365 (1977).
[32]B. Tatischeff, I. Brissaud, and L. Bimbot, Phys. Rev. C 5, 234 (1972); I. Brissaud, Y. Le Bornec, B. Tatischeff, L. Bimbot, M. K. Brussel, and G. Duhamel, Nucl. Phys. A191, 145 (1972).
[33]J. C. Lombardi, R. N. Boyd, R. Arking, and A. B. Robbins, Nucl. Phys. A188, 103 (1972).
[34]In order to extract the numbers in the table from the published numbers in Ref. 30 we have assumed that $\langle r_p^2\rangle^{1/2} = 3.487$ fm and $\langle r_N^2\rangle^{1/2} = 3.477$ fm for ^{40}Ca.
[35]H. O. Meyer, Phys. Rev. C 17, 1116 (1978).